Electrochemiluminescence Amplification in Bead-Based Assays Induced by a Freely Diffusing Iridium(III) Complex

Electrochemiluminescence amplification in bead-based assays induced by a freely diffusing iridium(III) complex

Emily Kerr[1,*], Sara Knezevic[2], Paul S. Francis[3], Conor F. Hogan[4], Giovanni Valenti[5], Francesco Paolucci[5], Frédéric Kanoufi[6], Neso Sojic[2,*]

[1] Institute for Frontier Materials, Deakin University, Geelong, Victoria 3220, Australia.

[2] Univ. Bordeaux, CNRS, Bordeaux INP, Institut des Sciences Moléculaires, UMR 5255, 16 avenue Pey-Berland, 33607 Pessac, France.

[3] School of Life and Environmental Sciences, Deakin University, Geelong, Victoria 3220, Australia.

[4] Department of Biochemistry and Chemistry, Biomedical and Environmental Sensor Technology Centre, La Trobe Institute for Molecular Science, La Trobe University, Melbourne, Victoria 3086, Australia.

[5] Department of Chemistry "Giacomo Ciamician", University of Bologna, 40126 Bologna, Italy.

[6] Université Paris Cité, ITODYS, CNRS, F-75013 Paris, France

Corresponding Authors. Emails: emily.kerr@deakin.edu.au ; sojic@u-bordeaux.fr

KEYWORDS: Electrochemiluminescence, Imaging, Bead-based assays, Heterogeneous assays, Electrochemistry

ABSTRACT: Heterogeneous electrochemiluminescence (ECL) assays employing tri-*n*-propylamine as a co-reactant and a tris(2,2′-bipyridine)ruthenium(II) ($[Ru(bpy)_3]^{2+}$) derivative as an emissive label are integral to the majority of academic and commercial applications of ECL sensing. This model system is an active research area and constitutes the basis of successfully commercialized bead-based ECL immunoassays. Herein, we propose a novel approach to the enhancement of such conventional ECL assays *via* the incorporation of a second metal coordination complex, $[Ir(sppy)_3]^{3-}$ (where sppy = 5′-sulfo-2-phenylpyridinato-C^2,N), to the experimental system. By employing ECL microscopy we are able to map the spatial distribution of ECL emission at the surface of the bead, from $[Ru(bpy)_3]^{2+}$ labels, and solution-phase emission, from $[Ir(sppy)_3]^{3-}$. The developed $[Ir(sppy)_3]^{3-}$-mediated enhancement approach elicited a significant improvement (70.9-fold at 0.9 V and 2.9-fold at 1.2 V) of the ECL signal from $[Ru(bpy)_3]^{2+}$ labels immobilized on the surface of a polystyrene bead. This dramatic enhancement in ECL signal, particularly at low-oxidation potentials, has important implications for the improvement of existing heterogeneous ECL assays and ECL-based microscopy, by amplifying the signal, opening new bioanalytical detection schemes, and reducing both electrode surface passivation and deleterious side reactions.

Electrogenerated chemiluminescence or electrochemiluminescence (ECL) is the process by which highly reactive intermediates, generated by an applied electrochemical potential, react to form excited states of a luminophore.[1, 2] The development of ECL has led to a plethora of analytical applications in aqueous environments in both academic publications and commercial instrumentation.[2-5] ECL has numerous advantages when compared to alternative signal generation strategies (such as fluorescence and electrochemistry), owing to the separation of the signal generation (electrochemical) and detection (spectroscopic) techniques. Furthermore, ECL allows precise temporal control of the reaction processes, low background and wide dynamic range.[6, 7] Despite its

advantages, ECL remains an intrinsically surface-confined process that incorporates concomitant steps to generate the emission, of which optimization may lead to a significant increase of the analytical signal.[8-13] Herein, we explore a novel strategy to enhance the ECL signal mediated by a freely-diffusing Ir(III) coordination complex.[9, 14-16]

To undertake bioanalytical ECL sensing in aqueous environments, researchers employ a 'co-reactant': a sacrificial species that, after oxidation or reduction, forms a strongly reducing or oxidizing intermediate that reacts with the luminophore.[2, 4, 5, 17, 18] The majority of analytical applications of ECL sensing employ tris(2,2'-bipyridine)ruthenium(II) ($[Ru(bpy)_3]^{2+}$) as the emissive luminophore with tri-*n*-propylamine (TPrA) as a co-reactant.[5] Researchers have demonstrated various approaches to enhance the ECL from the $[Ru(bpy)_3]^{2+}$ and TPrA system including alternative labels, co-reactants or electrode materials, optimizing buffer conditions, and the addition of reagents such as surfactants.[5, 12, 13, 19-24] However, $[Ru(bpy)_3]^{2+}$ and TPrA remains the gold standard system for analytical applications of ECL.[1, 2, 4, 5, 8]

The ECL system at the basis of the design and operation of commercially available ECL instrumentation comprises $[Ru(bpy)_3]^{2+}$ luminophores constrained at the electrode surface (e.g., on magnetic beads) with freely diffusing TPrA. Approximately two billion bead-based ECL immunoassays for the detection of biomarkers in body fluids are conducted worldwide each year.[3] The Cobas (commercialized by Roche Diagnostics) system is a popular benchtop pathology instrument that, coupled with Elecsys immunoassays, enables the sensitive, rapid and specific detection of over 100 different biomarkers for *in-vitro* diagnostics.[3] Elecsys immunoassays predominantly

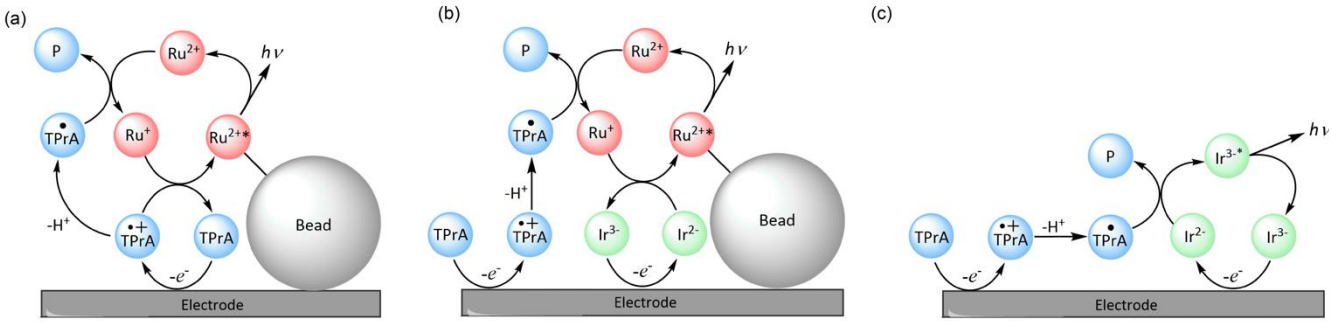

Figure 1: Schematics of (a) the conventional heterogeneous ECL route, (b) the redox-mediated ECL enhanced route in a heterogeneous bead-based ECL sensor format, and (c) homogeneous ECL from $[Ir(sppy)_3]^{3-}$ *via* the direct pathway. Ru^{2+} and Ir^{3-} represent the $[Ru(bpy)_3]^{2+}$ derivative used as an ECL label (denoted below as Ru@PS) decorating the micrometric bead and the $[Ir(sppy)_3]^{3-}$ redox mediator, respectively.

employ a classic sandwich immunoassay design; a detection antibody is labelled with a $[Ru(bpy)_3]^{2+}$ derivative and a second antibody is labelled with a biotin group. These antibodies are combined with the analyte containing biological sample and allowed to form an immuno-complex, then mixed with streptavidin coated magnetic microparticles. The immuno-complex-modified magnetic beads are subsequently injected into an electrochemical cell with the working electrode positioned over a magnet to capture the magnetic particles.[3] An electrochemical potential is applied to the cell and the resulting ECL from the $[Ru(bpy)_3]^{2+}$ label is captured using a photomultiplier tube positioned above the flow-cell; the intensity of the ECL signal is proportional to the analyte concentration.[3]

Such assays – where the ECL labels are immobilized on an insulating object (such as a bead or cell) and the co-reactant is freely diffusing in solution – are termed 'heterogeneous', as opposed to homogeneous (solution-phase) systems. In homogeneous ECL process where both $[Ru(bpy)_3]^{2+}$ and TPrA are diffusing in solution, several competitive mechanistic pathways may occur (Scheme S1).[6, 25] The heterogeneous mechanism (also known as the 'remote', 'revisited' or 'indirect' route; Figure 1a and Scheme S2) also plays an essential role in ECL microscopy of single entities such as cells or organelles.[12, 26-30] The critical impact of the design of such heterogeneous assays is that only the co-reactant can diffuse to the electrode surface to undergo oxidation owing to the majority of labels being outside of direct electron tunneling distance (~1-2 nm) and too far away from the electrode surface to undergo direct oxidation.[25]

Due to the widespread uptake and popularity of heterogeneous ECL immunoassays, extensive research has been conducted on the $[Ru(bpy)_3]^{2+}$ and TPrA bead-based immunoassay to determine the critical parameters of the system.[2, 4-6, 11, 12, 17, 21, 25, 27, 31-33] ECL microscopy has allowed researchers to make significant improvements in the analytical sensitivity of conventional heterogeneous ECL assays.[32] For example, Dutta et al. developed a novel strategy to minimize variation between successive ECL measurements by examining a heterogeneous bead-based assay using ECL microscopy.[31] The researchers demonstrated that by applying a series of negative regenerative pulses to the working electrode, electrode passivation by TPrA could be minimized, thereby improving the repeatability and accuracy of the technique.[31] Zanut et al. used ECL microscopy as a tool to investigate and demonstrate the use of a new additive co-reactant

N-dipropyl isobutyl amine (DPIBA).[12] The addition of DPIBA to a conventional heterogeneous ECL assay enabled signal enhancements of up to 128%.[12]

Proof-of-concept homogeneous ECL experiments are frequently used to demonstrate improvements in analytical sensing prior to the incorporation in a heterogeneous assay. Recently, Kerr et al. proposed a novel method of enhancing homogeneous ECL from the $[Ru(bpy)_3]^{2+}$ and TPrA system *via* the incorporation of $[Ir(sppy)_3]^{3-}$ (where sppy = 5′-sulfo-2-phenylpyridinato-C^2,*N*, Figure S1) to the experimental solution.[9, 14, 15] Enhancement of ECL from $[Ru(bpy)_3]^{2+}$ by up to 10.8-fold was observed with the addition of a $[Ir(sppy)_3]^{3-}$ at potentials (0.9 V) where $[Ru(bpy)_3]^{2+}$ is not oxidized (1.1 V *vs* Ag/AgCl, Figure S2). Considering the spectral properties of the two luminophores (Figure S3), the energy transfer pathway is disfavored. Hence, the authors proposed a redox-mediated ECL enhancement pathway, outlined in Figure 1b and Scheme S3. Initially $[Ru(bpy)_3]^{2+}$ is reduced by $TPrA^{\bullet}$ to form $[Ru(bpy)_3]^{+}$ (reaction 4). In addition to its reaction with $TPrA^{\bullet+}$, $[Ru(bpy)_3]^{+}$ may also react with $[Ir(sppy)_3]^{2-}$ (produced *via* direct oxidation of $[Ir(sppy)_3]^{3-}$ at the electrode surface), to form $[Ru(bpy)_3]^{2+*}$ and undergo subsequent radiative decay.[14]

Herein, we evaluate this $[Ir(sppy)_3]^{3-}$-mediated enhancement strategy in a bead-based format using ECL microscopy to determine if this pathway translates to increased ECL signals in a model heterogeneous ECL assay. Furthermore, we demonstrate that previously observed enhancement of ECL from $[Ru(bpy)_3]^{2+}$ at low oxidation potentials in homogeneous ECL experiments translates to enhancement in a heterogeneous assay, which has particular promise for improving the sensitivity and reproducibility of analytical ECL systems.[14] Finally, we demonstrate the versatility of the $[Ir(sppy)_3]^{3-}$-mediated ECL enhancement approach by examining an alternative co-reactant, 2-(dibutylamino)ethanol (DBAE).[20]

RESULTS AND DISCUSSION

To examine the effect of the dissolved $[Ir(sppy)_3]^{3-}$ mediator on heterogeneous bead-based ECL assays, we used covalently labelled 12 µm PS beads functionalized with a $[Ru(bpy)_3]^{2+}$ derivative (denoted Ru@PS beads) as a model system (Figures 1, 2). Previous research has demonstrated that the ECL observed in such an Ru@PS bead system is an accurate model for that of a heterogeneous bead-based ECL sandwich immunoassay.[31, 32, 34, 35] Both photoluminescence (PL) and ECL micrographs (Figure 2) of single Ru@PS beads exhibited a typical pattern for top-view microscopy experiments

(Figure S4). ECL profiles were determined using ImageJ software; a detailed image analysis procedure is provided in the SI.

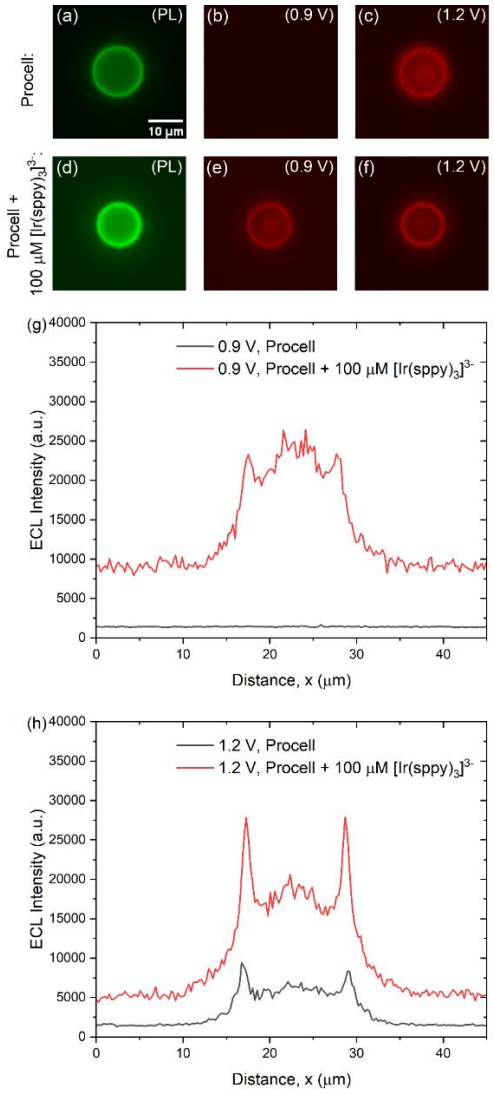

Figure 2: Representative micrographs, top-view configuration, of single 12 µm Ru@PS beads using PL (a and d, contrast scale 0 to 65,000) and ECL mode (b and c contrast scale 0 to 12,000, e and f contrast scale 0 to 45,000). Figures a-c obtained in Procell, d-f obtained in Procell with 100 µM $[Ir(sppy)_3]^{3-}$. Figures b and e: 0.9 V, figures c and f: 1.2 V. Representative profiles of ECL intensity of Ru@PS beads at 0.9 V (g, extracted from images b and e) and 1.2 V (h, extracted from images c and f) in Procell without and with 100 µM $[Ir(sppy)_3]^{3-}$.

PL micrographs showed uniform distribution of $[Ru(bpy)_3]^{2+}$ labels but in ECL micrographs, non-uniform emission was instead observed across the surface of the bead. The pattern of ECL recorded in top-view experiments – with bright ECL at the center and edges of the bead – is primarily due to the optical pathway through the PS bead.[32] The ECL from Ru@PS beads in Procell solution at 0.9 V, below the oxidation potential of $[Ru(bpy)_3]^{2+}$ ($E^{0\prime}$ = 1.1 V vs Ag/AgCl) but above the oxidation potential of TPrA ($E^{0\prime} \approx$ 0.83-0.95 V vs Ag/AgCl)[25, 36, 37] was barely visible (Figure 2b). However, the addition of 100 µM $[Ir(sppy)_3]^{3-}$ to the

Procell solution, beside contributing to an overall increase of the background luminosity (due to the Ir-based homogeneous ECL, *vide infra*), brought about a clear enhancement of the ECL from the Ru@PS beads (Figure 2e). At 1.2 V, the ECL from both the conventional and $[Ir(sppy)_3]^{3-}$-mediated systems were visible due to the increased availability of electro-oxidized TPrA radicals at this potential (Figure S2). However, the ECL from Ru@PS was significantly brighter with the addition of 100 µM $[Ir(sppy)_3]^{3-}$ (Figures 2c and 2f).

To obtain a quantitative representation of the ECL emission, we extracted the ECL profile (Figure 2g and 2h) from each image. The significant increase in the background ECL when 100 µM $[Ir(sppy)_3]^{3-}$ was added to the solution results from ECL emission from $[Ir(sppy)_3]^{3-}$*; generated *via* the direct pathway with TPrA (Figure 1c). To examine the effect of the addition of $[Ir(sppy)_3]^{3-}$ on the ECL from the $[Ru(bpy)_3]^{2+}$ derivative labels, we subtracted the background ECL from the raw profiles (as detailed in Figure S5) and calculated the maximum ECL intensity from the resulting background-subtracted profile which was attributed only to emission from Ru@PS. When 100 µM $[Ir(sppy)_3]^{3-}$ was added to the experimental system, we observed a dramatic 70.9-fold enhancement of ECL from the Ru@PS beads at 0.9 V and a 2.9-fold enhancement at 1.2 V (Figure 3). Both values were significantly higher than the ECL enhancement observed in the previous corresponding solution-phase experiments (10.8-fold and 1.5-fold in solution-phase respectively).[14]

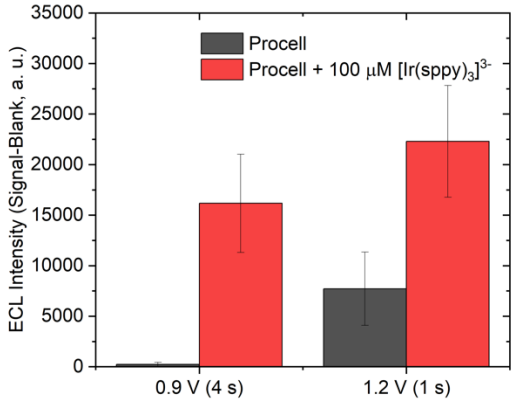

Figure 3: ECL intensities, top-view configuration, n = 6 electrodes, in Procell (grey columns) and Procell with 100 µM $[Ir(sppy)_3]^{3-}$ (red columns) at 0.9 V and 1.2 V. Same experimental conditions as in Figure 2.

The reported approach provides a new strategy for the production of bright ECL signals in the heterogeneous format, which opens new possibilities for ECL sensing and imaging. The ability to conduct ECL at low oxidation potentials is particularly important for biosensors and cell imaging, where high potentials can cause (i) oxygen evolution reaction (i.e. bubbles at the electrode surface), (ii) ECL background emission, (iii) damage to

biological recognition elements or cleavage of the biological recognition elements from solid supports, and (iv) damage to the microfabricated electrode in miniaturized sensing systems due to high currents and/or potentials.[10, 38-40] Furthermore, recent research has demonstrated that the application of high potentials in ECL experiments can lead to an increase in electrode passivation and deleterious side reactions, both of which decrease the analytical sensitivity of the technique.[28, 31] The advantage of being able to conduct ECL at low oxidation potentials, combined with the signal enhancement observed in the $[Ir(sppy)_3]^{3-}$-mediated heterogeneous model assay when compared to the standard $[Ru(bpy)_3]^{2+}$ and TPrA system, indicate the promise of this strategy for the development of ultra-sensitive heterogeneous ECL assays.

To further investigate the effects of adding 100 µM $[Ir(sppy)_3]^{3-}$ to the ECL system, we used an orthogonal side-view configuration (Figure S4) which can yield information on the width of the ECL emitting layer (i.e., how far away from the electrode surface ECL can be observed). Considerable research has been conducted in recent years to precisely define and modify the thickness of the ECL emitting layer.[21, 32, 33, 35, 41] The stability of the $TPrA^{\bullet+}$ is a determining factor.[12, 25, 32] Fiorani et al. demonstrated that by modifying the buffer concentration, the deprotonation rate of $TPrA^{\bullet+}$ (Scheme S1, reaction 4) could be controlled, enabling the modulation of the concentration profiles of both $TPrA^{\bullet}$ and $TPrA^{\bullet+}$ in the experimental solution and, therefore, the precise modulation of the thickness of the ECL emission layer.[21, 42] This approach enables both the improvement of the ECL signal in conventional systems and the examination of substrates of different heights.[21] Furthermore, researchers have exploited the catalytic ECL route to significantly extend the ECL emitting layer, owing to the comparatively high stability of the $[Ru(bpy)_3]^{3+}$ species when compared to $TPrA^{\bullet+}$.[33, 41] Based on this research, it could be reasonably hypothesized that the comparatively high stability of the $[Ir(sppy)_3]^{2-}$ species might induce a similar increase in the length of the ECL emissive layer. However, the high local concentration and reactivity of both TPrA radicals should also be considered because they confine the ECL reaction at the electrode surface due to their short lifetimes. Side-view ECL microscopy (Figure S4) allows the examination of this phenomenon in the $[Ir(sppy)_3]^{3-}$-mediated ECL system (Figure 4). These micrographs showed a typical side-view profile, with two visible ECL emitting regions, one close to the electrode surface, due to ECL emission from Ru@PS, and the second at the top of the bead, due to the optical paths

and focusing effect of the bead as previously described.[32] The reflection of the bead on the electrode surface was also clearly visible in both the PL and ECL profiles (Figure 4e); ECL emissions at positive z values (z > 0) result from luminophores in the solution ($[Ir(sppy)_3]^{3-}$*) or on the bead ($[Ru(bpy)_3]^{2+}$*) and those at negative z values (z < 0) result from the reflection of ECL on the electrode surface. Interestingly, when 100 µM $[Ir(sppy)_3]^{3-}$ was added to the solution, a distinct 'shadow' region from ~1.6 to 4.4 µm from the electrode surface was visible in the ECL micrograph (Figure 4d). This visual effect is, however, attributed to an artifact, likely resulting from tilting of the microscope objective with respect to the bead, which may cause the lower half of the bead to be slightly more visible than the upper half. Furthermore, the bead modifies the pathway of photons emitted by $[Ir(sppy)_3]^{3-}$ luminophores located behind the bead, which propagate through the bead *via* complex refraction pathways that may alter the emission profile. Outside of the range of the bead the EM-CCD collects all ECL emission from $[Ir(sppy)_3]^{3-}$ luminophores within the depth of field centered at the focal plane and this effect, combined with the altered angle of the microscope objective relative to the Ru@PS bead, may explain the observed shadow region. The combined effects of bead blocking and the tilting of the microscope objective may explain the observed shadow region. This was supported by examination of the ECL of bare (unlabeled) PS beads (Figure S6).

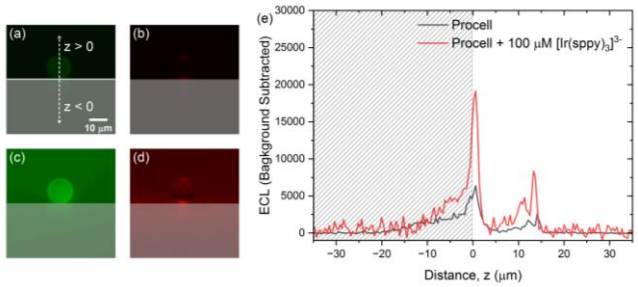

Figure 4: Micrographs, side-view configuration, of 12 µm Ru@PS beads using PL (a and c) and ECL mode (b and d), contrast scale 0 to 30,000. Solid horizontal line in (a) represents the electrode surface, intersecting dashed line represents ECL profile with emission at values of z > 0 resulting from ECL from Ru@PS or $[Ir(sppy)_3]^{3-}$ in solution and emission at values of z < 0 resulting from the reflection of ECL at the surface of the glassy carbon working electrode (represented by the shaded zone in each micrograph). Figures a-b obtained in Procell, c-d obtained in Procell with 100 µM $[Ir(sppy)_3]^{3-}$. Representative background subtracted (as described in SI and Figure S6) profiles of ECL intensity of Ru@PS beads at 1.2 V in Procell without and with 100 µM $[Ir(sppy)_3]^{3-}$. The hatched zone represents reflection of ECL on the electrode surface (i.e. z < 0 µm).

After accounting for both the blocking effect of the bare beads and the angle of the objective, side-view profiles revealed that there is no significant extension in the ECL emissive layer in Procell solutions when $[Ir(sppy)_3]^{3-}$ is added to the solution (Figure 4, Figure S7b). This could result from inaccuracies in the method of correction for the blocking effect of the beads (Figure S6) or the fact that the high concentration of

phosphate buffer in Procell (0.3 M) limits the lifetime of $TPrA^{\bullet+}$ and, therefore, $TPrA^{\bullet}$ into the solution, restricting the distance from the electrode at which reactions 12 and 13 (Scheme S2) can occur which are essential for ECL emission *via* the heterogeneous pathway.[21] Despite there being no significant change in the distance-dependent profile of the ECL emission with the addition of $[Ir(sppy)_3]^{3-}$, significant enhancement of the ECL signal from Ru@PS is also observed in the side-view configuration (2.4-fold, Figure S7a). This enhancement is consistent with the results obtained in the top-view configuration (*vide supra*). The similar ECL patterns and the limited extension of the ECL-emitting region observed with and without $[Ir(sppy)_3]^{3-}$ suggest that radiative energy transfer between $[Ir(sppy)_3]^{3-*}$ and Ru@PS is not the dominant process occurring in the heterogeneous bead-based format. It is important to note that, in addition to the previously proposed redox-mediated pathway (Figure 1b), catalytic generation of $TPrA^{\bullet+}$ by electro-oxidized $[Ir(sppy)_3]^{2-}$ may also play a role in the ECL enhancement. However, to elucidate the contribution of each pathway to the observed enhancement, a comprehensive simulation of the underlying reaction pathways would be required, and such complete mechanistic studies are outside of the scope of this report.

Xu and co-workers first demonstrated homogeneous ECL of $[Ru(bpy)_3]^{2+}$ with DBAE, an alternative amine co-reactant (i.e. with both ECL reagents dissolved in solution).[20] The authors observed ~10 times higher ECL with DBAE as a co-reactant when compared to TPrA in the solution-phase system at gold electrodes.[20] However, when Sentic et al. examined DBAE as a co-reactant in a heterogeneous Ru@PS bead-based model, lower ECL from Ru@PS was observed when using DBAE compared to TPrA.[32] This was attributed to the poor (~10 times lower) stability of $DBAE^{\bullet+}$ when compared to $TPrA^{\bullet+}$, reducing the distance to which DBAE radicals can diffuse into the solution and decreasing the distance from the electrode surface at which ECL can occur.[32] Unlike the solution-phase system examined by Xu et al., where both the direct and the catalytic pathways may contribute to the ECL emission, such routes are unavailable in a heterogeneous bead-based system where the $[Ru(bpy)_3]^{2+}$ label is immobilized on the surface of a bead (Figure 1a) thus resulting in significantly weaker emissions.

When DBAE was combined with $[Ir(sppy)_3]^{3-}$, however, the ECL observed from Ru@PS was 3.1-fold higher when compared to DBAE alone at 1.2 V (Figures S8, S9). This would suggest that a similar $[Ir(sppy)_3]^{3-}$-mediated enhancement mechanism occurs with both TPrA and

DBAE as a co-reactant. However, as mentioned above, while the proposed redox-mediated ECL mechanism may contribute to the observed ECL enhancement, alternative mechanisms (such as radiative energy transfer and catalytic generation of $DBAE^{\bullet+}$ by electro-oxidized $[Ir(sppy)_3]^{2-}$) may play a role and the contribution of these pathways to the observed enhancement is currently under investigation. As a rule of thumb, the catalytic generation of both amine radical cations by electro-oxidized $[Ir(sppy)_3]^{2-}$ should compare with the values reported for the electro-oxidized $[Fe(bpy)_3]^{3+}$.[36] Indeed, both redox mediators have comparable $E^{0'}$ and from their similar ligand structure would have likely similar outer-sphere type self-exchange electron transfer. Expected values for the rate constant of this mediated electron transfer would be in the range of 10^4 to 10^5 M^{-1} s^{-1}, sufficient to explain the ECL enhancement at the $[Ir(sppy)_3]^{3-}$ oxidation potential (mediating the amine oxidation). It is important to note that the ECL intensity observed from the DBAE system was much lower than that observed in Procell; for DBAE a 15 s pulse time was needed to obtain a substantial ECL signal at 1.2 V, compared to 1 s for Procell. Similarly, the ECL from a heterogeneous ECL format was 7-fold lower when using DBAE as a co-reactant when compared to TPrA.[32] The consistency of the enhancement of ECL from Ru@PS with both TPrA and DBAE as a co-reactant demonstrates the versatility of the $[Ir(sppy)_3]^{3-}$-mediated ECL approach.

CONCLUSION

We present a new approach for the enhancement of $[Ru(bpy)_3]^{2+}$ ECL in a conventional, heterogeneous assay format where the $[Ru(bpy)_3]^{2+}$ labels are attached to micrometric beads, as in classic ECL bead-based immunoassays. The addition of $[Ir(sppy)_3]^{3-}$ to the experimental solution yielded a significant increase in ECL from the $[Ru(bpy)_3]^{2+}$ labels. This enhancement was particularly pronounced at low oxidation potentials (0.9 V vs Ag/AgCl), below the oxidation potential of $[Ru(bpy)_3]^{2+}$ (1.1 V vs Ag/AgCl). The ability to produce bright ECL signals at low oxidation potentials is particularly important for improving the versatility, sensitivity and reproducibility of heterogeneous ECL assays because the lower applied potential for analysis avoids the oxygen evolution reaction with the formation of bubbles and of local pH gradients. Moreover, it enables: (i) decrease of electrode surface passivation by TPrA, (ii) reduction of the incidence of interfering side reactions, (iii) ECL analysis at potentials lower than that required to cleave biological recognition elements that are covalently linked to the electrode surface, and (iv) the

creation of miniaturized ECL sensing devices by reducing current generation and subsequent electrode degradation. Finally, we demonstrate the versatility of the $[Ir(sppy)_3]^{3-}$-mediated ECL enhancement approach by examining the system using DBAE an alternative co-reactant. These results demonstrate that $[Ir(sppy)_3]^{3-}$ can induce enhancements of ECL from $[Ru(bpy)_3]^{2+}$ in different analytical systems. Finally, since the solution-phase ECL of the $[Ru(bpy)_3]^{2+}$ and TPrA system is widely used in imaging, the $[Ir(sppy)_3]^{3-}$-mediated pathway constitutes an appealing opportunity to develop ECL microscopy with improved sensitivity and increased complexity.

EXPERIMENTAL SECTION

All reagents and chemicals were purchased from Sigma-Aldrich and used as received unless otherwise specified. $Na_3[Ir(sppy)_3]$ was purchased from Lumtec. Procell M was purchased from Roche. Solutions were prepared in ultra-pure (Milli-Q) water unless otherwise specified. Amine-functionalized, 12 µm polystyrene (PS) beads purchased from Kisker Biotech GmbH & Co and functionalized using a previously described procedure.[32] Briefly, 10 µL of 2.5% PS beads were diluted in 1 mL of 1× phosphate buffered saline (PBS) and washed using centrifugation (10 min, 10,000 rpm) prior to resuspension in 1 mL of 1× PBS. 1 mg of bis(2,2'-bipyridine)-4'-methyl-4-carboxybipyridine-ruthenium *N*-succinimidyl ester bis(hexafluorophosphate) ($[Ru(bpy)_2(mbpy\text{-}NHS)]^{2+}$) was dissolved in 100 µL of dimethylsulfoxide and added to the suspension. This suspension was stirred for 3 h at 4°C. The resulting $[Ru(bpy)_3]^{2+}$ derivative functionalized PS beads *via* a peptide bond (noted Ru@PS) were washed 10 times using centrifugation, resuspended in 1 mL of 1× PBS, and stored at 4°C.

A custom-designed cell housed the working electrode (WE, 3 mm diameter, Teflon shrouded, glassy carbon), reference electrode (RE, Ag/AgCl, 3.5 M KCl) and counter electrode (CE, Pt wire). All potentials are referenced versus Ag/AgCl. A PalmSens potentiostat (Metrohm) was used for all electrochemical measurements. Working electrodes were prepared by drop casting a small volume (3-6 µL) of polystyrene beads in 1X PBS buffer onto the working electrode surface and allowing the solution to evaporate at room temperature in dark-room conditions. PL micrographs were collected using a FITC-LP filter (Leica, 11525302) of beads at the working electrode (WE) surface prior to applying an electrochemical potential. A single chronoamperometric (CA) pulse to the designated potential was applied to the WE (*vs* the RE potential), the length of the pulse

was varied to ensure the obtained signals were within the linear range of the EM-CCD detector: for top-view experiments in Procell a 4 s CA pulse to 0.9 V or a 1 s CA pulse to 1.2 V was used, for side-view experiments in Procell a 2 s CA pulse to 1.2 V was used, for experiments using DBAE as a co-reactant a 15 s CA pulse was used. An inverted Leica DMi8 microscope equipped with a Hamamatsu EM-CCD camera (C9100-23B) was used to collect the ECL emission for each pulse. The exposure time of the EM-CCD camera was set to 1 s longer than the aforementioned CA pulse time, to ensure all ECL emission was captured. A 63× objective (Leica, 11506279) was used for all top-view measurements and a 40× objective (Leica, 11506155) was used for all side-view measurements (Figure S4). Three consecutive measurements were collected at each WE and the ECL signal was calculated as an average response from the three consecutive measurements (Figure S10). ImageJ software was used for all micrograph analysis with detailed procedures included in the SI.

ASSOCIATED CONTENT

Supporting Information.
Supporting information includes image analysis strategies, reaction schemes, structures, cyclic voltammograms, UV-Vis and PL spectra and supplementary ECL microscopy results. This material is available free of charge via the Internet at http://pubs.acs.org.

ACKNOWLEDGMENT

E. K. gratefully acknowledges the National Health and Medical Research Council (NHMRC) of Australia (GNT1161573), the Victorian Government, Victorian Endowment for Science Knowledge and Innovation (VESKI) Victoria Fellowship, the Science and Industry Endowment Fund (SIEF) and Australian Academy of Science (AAS) SIEF-AAS Fellowship. This work was also supported by ARC Discovery grant DP200102947 and Agence Nationale de la Recherche (ELISE - ANR-21-CE42).

REFERENCES

1. Sojic, N., *Analytical electrogenerated chemiluminescence: from fundamentals to bioassays*. Royal Society of Chemistry: 2019; Vol. 15.
2. Hesari, M.; Ding, Z., Electrogenerated chemiluminescence: light years ahead. *J. Electrochem. Soc* **2016,** *163* (4), H3116-H3131.
3. Faatz, E.; Finke, A.; Josel, H.-P.; Prencipe, G.; Quint, S.; Windfuhr, M., Automated Immunoassays for the Detection of Biomarkers in Body Fluids. In *Analytical Electrogenerated Chemiluminescence: From Fundamentals to Bioassays*, Sojic, N., Ed. The Royal Society of Chemistry: 2020; pp 443-470.
4. Miao, W., Electrogenerated Chemiluminescence and its Biorelated Applications. *Chem. Rev.* **2008,** *108* (7), 2506-2553.
5. Kerr, E.; Doeven, E. H.; Francis, P. S., Recent advances in mechanistic understanding and analytical methodologies of the electrochemiluminescence of tris(2,2′-bipyridine)ruthenium(II) and tri-*n*-propylamine. *Curr. Opin. Electrochem.* **2022,** *35*, 101034.
6. Adsetts, J. R.; Chu, K.; Hesari, M.; Ma, J.; Ding, Z., Absolute Electrochemiluminescence Efficiency Quantification Strategy Exemplified with $Ru(bpy)_3^{2+}$ in the Annihilation Pathway. *Anal. Chem.* **2021,** *93* (33), 11626-11633.
7. Hesari, M.; Ding, Z., Spooling electrochemiluminescence spectroscopy: development, applications and beyond. *Nat. Protoc.* **2021,** *16* (4), 2109-2130.
8. Chu, K.; Adsetts, J. R.; Ma, J.; Zhang, C.; Hesari, M.; Yang, L.; Ding, Z., Physical Strategy to Determine Absolute Electrochemiluminescence Quantum Efficiencies of Coreactant Systems Using a Photon-Counting Photomultiplier Device. *J. Phys. Chem. C* **2021,** *125* (40), 22274-22282.
9. Kerr, E.; Doeven, E. H.; Barbante, G. J.; Hogan, C. F.; Hayne, D. J.; Donnelly, P. S.; Francis, P. S., New perspectives on the annihilation electrogenerated chemiluminescence of mixed metal complexes in solution. *Chem. Sci.* **2016,** *7* (8), 5271-5279.
10. Kirschbaum-Harriman, S.; Mayer, M.; Duerkop, A.; Hirsch, T.; Baeumner, A. J., Signal enhancement and low oxidation potentials for miniaturized ECL biosensors via N-butyldiethanolamine. *Analyst* **2017,** *142* (13), 2469-2474.
11. Lu, L.; Liu, C.; Kang, T.; Wang, X.; Guo, G.; Miao, W., In situ enhanced electrochemiluminescence based on co-reactant self-generated for sensitive detection of microRNA. *Sens. Actuat. B* **2018,** *255*, 35-41.
12. Zanut, A.; Fiorani, A.; Canola, S.; Saito, T.; Ziebart, N.; Rapino, S.; Rebeccani, S.; Barbon, A.; Irie, T.; Josel, H.-P.; Negri, F.; Marcaccio, M.; Windfuhr, M.; Imai, K.; Valenti, G.; Paolucci, F., Insights into the mechanism of coreactant electrochemiluminescence facilitating enhanced bioanalytical performance. *Nat. Commun.* **2020,** *11* (1), 2668.
13. Swanick, K. N.; Ladouceur, S.; Zysman-Colman, E.; Ding, Z., Self-Enhanced Electrochemiluminescence of an Iridium(III) Complex: Mechanistic Insight. *Angew. Chem. Int. Ed.* **2012,** *51* (44), 11079-11082.
14. Kerr, E.; Hayne, D. J.; Soulsby, L. C.; Bawden, J. C.; Blom, S. J.; Doeven, E. H.; Henderson, L. C.; Hogan, C. F.; Francis, P. S., A redox-mediator

pathway for enhanced multi-colour electrochemiluminescence in aqueous solution. *Chem. Sci.* **2022,** *13* (2), 469-477.
15. Kerr, E.; Doeven, E. H.; Barbante, G. J.; Hogan, C. F.; Bower, D. J.; Donnelly, P. S.; Connell, T. U.; Francis, P. S., Annihilation electrogenerated chemiluminescence of mixed metal chelates in solution: modulating emission colour by manipulating the energetics. *Chem. Sci.* **2015,** *6* (1), 472-479.
16. Soulsby, L. C.; Hayne, D. J.; Doeven, E. H.; Wilson, D. J. D.; Agugiaro, J.; Connell, T. U.; Chen, L.; Hogan, C. F.; Kerr, E.; Adcock, J. L.; Donnelly, P. S.; White, J. M.; Francis, P. S., Mixed annihilation electrogenerated chemiluminescence of iridium(III) complexes. *Phys. Chem. Chem. Phys.* **2018,** *20* (28), 18995-19006.
17. Miao, W.; Bard, A. J., Electrogenerated chemiluminescence. 72. Determination of immobilized DNA and C-reactive protein on Au(111) electrodes using tris(2,2'-bipyridyl)ruthenium(II) labels. *Anal. Chem.* **2003,** *75* (21), 5825-5834.
18. Miao, W.; Choi, J.-P., Coreactants. In *Electrogenerated Chemiluminescence*, Bard, A. J., Ed. Marcel Dekker Inc: New York, 2004; pp 213-271.
19. Xu, G.; Pang, H.-L.; Xu, B.; Dong, S.; Wong, K.-Y., Enhancing the electrochemiluminescence of tris(2,2′-bipyridyl)ruthenium(II) by ionic surfactants. *Analyst* **2005,** *130* (4), 541-544.
20. Liu, X.; Shi, L.; Niu, W.; Li, H.; Xu, G., Environmentally Friendly and Highly Sensitive Ruthenium(II) Tris(2,2′-bipyridyl) Electrochemiluminescent System Using 2-(Dibutylamino)ethanol as Co-Reactant. *Angew. Chem. Int. Ed.* **2007,** *46* (3), 421-424.
21. Fiorani, A.; Han, D.; Jiang, D.; Fang, D.; Paolucci, F.; Sojic, N.; Valenti, G., Spatially resolved electrochemiluminescence through a chemical lens. *Chem. Sci.* **2020,** *11* (38), 10496-10500.
22. Fernandez-Hernandez, J. M.; Longhi, E.; Cysewski, R.; Polo, F.; Josel, H.-P.; De Cola, L., Photophysics and Electrochemiluminescence of Bright Cyclometalated Ir(III) Complexes in Aqueous Solutions. *Anal. Chem.* **2016,** *88* (8), 4174-4178.
23. Swanick, K. N.; Ladouceur, S.; Zysman-Colman, E.; Ding, Z., Bright electrochemiluminescence of iridium(iii) complexes. *Chem. Commun.* **2012,** *48* (26), 3179-3181.
24. Swanick, K. N.; Sandroni, M.; Ding, Z.; Zysman-Colman, E., Enhanced Electrochemiluminescence from a Stoichiometric Ruthenium(II)–Iridium(III) Complex Soft Salt. *Chem. Eur. J.* **2015,** *21* (20), 7435-7440.
25. Miao, W.; Choi, J.-P.; Bard, A. J., Electrogenerated Chemiluminescence 69: The Tris(2,2'-bipyridine)ruthenium(II), ($Ru(bpy)_3^{2+}$)/Tri-*n*-propylamine (TPrA) System Revisited A New Route Involving $TPrA^{\bullet+}$ Cation Radicals. *J. Am. Chem. Soc.* **2002,** *124* (48), 14478-14485.
26. Ma, Y.; Colin, C.; Descamps, J.; Arbault, S.; Sojic, N., Shadow Electrochemiluminescence Microscopy of Single Mitochondria. *Angew. Chem. Int. Ed.* **2021,** *60* (34), 18742-18749.
27. Zhang, J.; Arbault, S.; Sojic, N.; Jiang, D., Electrochemiluminescence Imaging for Bioanalysis. *Ann. Rev. Anal. Chem.* **2019,** *12* (1), 275-295.
28. Fiorani, A.; Valenti, G.; Irkham; Paolucci, F.; Einaga, Y., Quantification of electrogenerated chemiluminescence from tris(bipyridine)ruthenium(ii) and hydroxyl ions. *Phys. Chem. Chem. Phys.* **2020**.
29. Voci, S.; Goudeau, B.; Valenti, G.; Lesch, A.; Jović, M.; Rapino, S.; Paolucci, F.; Arbault, S.; Sojic, N., Surface-Confined Electrochemiluminescence Microscopy of Cell Membranes. *J. Am. Chem. Soc.* **2018,** *140* (44), 14753-14760.
30. Han, D.; Goudeau, B.; Manojlovic, D.; Jiang, D.; Fang, D.; Sojic, N., Electrochemiluminescence Loss in Photobleaching. *Angew. Chem. Int. Ed.* **2021,** *60* (14), 7686-7690.
31. Dutta, P.; Han, D.; Goudeau, B.; Jiang, D.; Fang, D.; Sojic, N., Reactivity mapping of luminescence in space: Insights into heterogeneous electrochemiluminescence bioassays. *Biosens. Bioelectron.* **2020,** *165*, 112372.
32. Sentic, M.; Milutinovic, M.; Kanoufi, F.; Manojlovic, D.; Arbault, S.; Sojic, N., Mapping electrogenerated chemiluminescence reactivity in space: mechanistic insight into model systems used in immunoassays. *Chem. Sci.* **2014,** *5* (6), 2568-2572.
33. Guo, W.; Zhou, P.; Sun, L.; Ding, H.; Su, B., Microtube Electrodes for Imaging the Electrochemiluminescence Layer and Deciphering the Reaction Mechanism. *Angew. Chem. Int. Ed.* **2021,** *60* (4), 2089-2093.
34. Deiss, F.; LaFratta, C. N.; Symer, M.; Blicharz, T. M.; Sojic, N.; Walt, D. R., Multiplexed Sandwich Immunoassays Using Electrochemiluminescence Imaging Resolved at the Single Bead Level. *J. Am. Chem. Soc.* **2009,** *131* (17), 6088-6089.
35. Han, D.; Goudeau, B.; Lapeyre, V.; Ravaine, V.; Jiang, D.; Fang, D.; Sojic, N., Enhanced electrochemiluminescence at microgel-functionalized beads. *Biosens. Bioelectron.* **2022,** *216*, 114640.
36. Kanoufi, F.; Zu, Y.; Bard, A. J., Homogeneous Oxidation of Trialkylamines by Metal Complexes and Its Impact on Electrogenerated Chemiluminescence in the Trialkylamine/$Ru(bpy)_3^{2+}$ System. *J. Phys. Chem. B* **2001,** *105* (1), 210-216.
37. Lai, R. Y.; Bard, A. J., Electrogenerated Chemiluminescence. 70. The Application of ECL to Determine Electrode Potentials of Tri-*n*-propylamine, Its Radical Cation, and Intermediate Free Radical in MeCN/Benzene Solutions. *J. Phys. Chem. A* **2003,** *107* (18), 3335-3340.
38. Rodríguez, M. C.; Rivas, G. A., Label-free electrochemical aptasensor for the detection of lysozyme. *Talanta* **2009,** *78* (1), 212-216.
39. Liu, D.-Y.; Xin, Y.-Y.; He, X.-W.; Yin, X.-B., A sensitive, non-damaging electrochemiluminescent aptasensor via a low potential approach at DNA-modified gold electrodes. *Analyst* **2011,** *136* (3), 479-485.
40. Senthil Kumar, S.; Bard, A. J., Background Emission of Electrogenerated Chemiluminescence during Oxidation of Tri-*n*-propylamine from the Dimeric $^1\Delta_g$ State of O_2. *Anal. Chem.* **2013,** *85* (1), 292-295.
41. Ma, C.; Wang, M.-X.; Wei, H.-F.; Wu, S.; Zhang, J.-R.; Zhu, J.-J.; Chen, Z., Catalytic route electrochemiluminescence microscopy of cell membranes with nitrogen-doped carbon dots as nano-coreactants. *Chem. Commun.* **2021,** *57* (17), 2168-2171.
42. Daviddi, E.; Oleinick, A.; Svir, I.; Valenti, G.; Paolucci, F.; Amatore, C., Theory and Simulation for Optimising Electrogenerated Chemiluminescence from Tris(2,2′-bipyridine)-ruthenium(II)-Doped Silica Nanoparticles and Tripropylamine. *ChemElectroChem* **2017,** *4* (7), 1719-1730.

Graphic for manuscript